

Electroexcitation of giant multipole resonances in ^{24}Mg

K. Itoh

Saskatchewan Accelerator Laboratory, University of Saskatchewan, Saskatoon S7N 0W0, Canada

S. Ohsawa,* Y. Torizuka, T. Saito, and T. Terasawa

Laboratory of Nuclear Science, Tohoku University, Mikamine, Sendai, Japan 982

(Received 18 August 1980)

Highly excited multipole resonances of ^{24}Mg between 9 and 34 MeV excitation energy have been investigated by inelastic electron scattering for incident energies in the 102 and 200 MeV range. Prominent giant dipole resonances were observed at 18.9 and 20 MeV excitation energy, with a shape which is very similar to the shape of the photon-neutron cross section. Over twenty-five quadrupole and twenty octupole resonances were identified and separated by means of the multipole expansion method. The giant dipole strength exhausts $(85 \pm 17)\%$ of the isovector dipole energy-weighted sum rule. The quadrupole and the octupole strength exhaust $(117 \pm 23)\%$ and $(115 \pm 23)\%$ of the corresponding isoscalar energy-weighted sum rule, respectively. Evidence for the excitation of higher multipole states such as hexadecapole transitions was also found in the excitation energy region studied.

NUCLEAR REACTIONS $^{24}\text{Mg}(e, e')$, $E = 102, 125, 150, 200$ MeV, $q = 0.37-1.3$ fm $^{-1}$, measured $\sigma(E', \theta)$ up to 34 MeV in excitation energy; deduced dipole, quadrupole, and octupole strengths in giant resonance region. Enriched targets.

I. INTRODUCTION

The isoscalar giant quadrupole resonance (GQR) in sd -shell nuclei has attracted much attention recently because of its spreading character, which is in contrast to medium and heavy nuclei where the isoscalar GQR are well concentrated at $63/A^{1/3}$ MeV.^{1,2} The spreading of the GQR at energies below $63/A^{1/3}$ MeV for nuclei with a mass number $A < 40$ has been previously studied by means of radiative capture reactions of α particles.^{2,3} The strength was found to exhaust about half of the energy-weighted sum rule (EWSR).

The GQR in sd -shell nuclei has been extensively studied by α -particle scattering.⁴⁻⁷ Although at an early stage of the experiments it was reported that the GQR were too diffused to be observable,⁴ later measurement with 150 MeV α particles and with a resolution of 350–650 keV revealed a concentration of the GQR at $63/A^{1/3}$ MeV in sd -shell nuclei such as $^{20,22}\text{Ne}$ and ^{28}Si .⁵ Similar studies on magnesium isotopes⁶ have shown a splitting of the quadrupole strength. Such fragmentation was confirmed⁷ more recently by an α -particle scattering experiment at an overall energy resolution of 100 keV, and a splitting of the quadrupole resonance into several states or clusters of states was observed. In the adjacent nucleus ^{20}Ne , not only were several quadrupole resonances observed below 17 MeV, but also broad structures of a quadrupole nature were found at higher excitation energies around 25 MeV ($\sim 63/A^{1/3}$ MeV) by the inelastic electron scattering.⁸

The excitation energy region up to 15 MeV of

^{24}Mg has, in addition, been investigated by (p, p') ,⁹ (α, α') ,¹⁰ $(^3\text{He}, ^3\text{He}')$,¹¹ and (e, e') (Ref. 12) reactions. All these experiments also show the fragmentation of the quadrupole resonance. In particular, inelastic proton scattering with a resolution of 16 keV revealed nineteen 2^+ states and thirteen 3^- states up to 13.5 MeV in excitation energy.⁹

Investigation of the octupole resonance is also quite an interesting subject. In the region of nuclei between $A = 66$ and $A = 197$, concentrated octupole resonances were observed in the α -particle scattering experiment.¹³ Located between 5 and 10 MeV ($\sim 30/A^{1/3}$ MeV), such resonances account for 15–20% of the isoscalar octupole EWSR. The recent (p, p') reaction⁹ studies on ^{24}Mg have, however, shown nine octupole states up to 13.5 MeV, an indication of the fragmentation of the octupole strength in sd -shell nuclei.

In this paper we report on our experimental study of the giant dipole, quadrupole, octupole, and higher multipole resonances in ^{24}Mg by inelastic electron scattering. The giant dipole resonance (GDR) of ^{24}Mg has been studied largely by means of (γ, n) reactions.^{14,15} Prominent peaks were observed at 18.8, 19.2, and 20.0 MeV using monochromatic photons.¹⁴ Since the (γ, n) cross section exhausts only 16% of the classical dipole sum rule,¹⁴ it may be expected that the (e, e') experiment would reveal other aspects of the GDR of ^{24}Mg . Other reported works on the (γ, p) and total photoabsorption measurements^{16,17} have been conducted on natural magnesium targets. The giant resonance region of ^{24}Mg has been measured by electron scattering at low momentum transfers.¹⁸

Twenty four resonances were reported in that work between the 14.6 and 25.0 MeV excitation energy region of ^{24}Mg .

II. EXPERIMENT

The experiment was performed at the Tohoku University 300-MeV Electron Linear Accelerator. Using the recently completed Energy Compression System,¹⁹ electron beams of several microamperes on target were obtained in this experiment. The targets were isotopically enriched (99.96%) self-supporting foils of ^{24}Mg with thicknesses of 7.42 mg/cm² (for an incident energy of 150 MeV) and 42.5 mg/cm² (for incident energies of 102, 125, and 200 MeV). Overall energy resolution full width at half-maximum (FWHM) was approximately 120 keV for the measurement at an incident energy of 150 MeV, and 200 keV for the measurement at 200 MeV. The excitation energies were determined within an accuracy of ± 50 keV. This was confirmed by comparing the well-known 15.11 MeV, 1^+ and 16.11 MeV, 2^+ levels of ^{12}C with the inelastic spectrum of ^{24}Mg at a fixed setting of the magnetic field of the spectrometer, thus avoiding the ambiguity arising from fluctuations of the magnetic field setting.

Inelastically scattered electrons were detected by a 100 cm radius double focusing magnetic spectrometer equipped with a 33-channel solid state detector system. Detailed descriptions of the detector system and its use have been published elsewhere.²⁰ The incident beam energies and scattering angles used were 150 MeV 30° , 40° , and 200 MeV 35° , 45° , 55° , 65° , 75° , and 85° . In order to investigate the transverse excitations,

spectra were also measured at a backward angle of 155° , with 102 and 125 MeV incident energies. These two energies were chosen so as to match the momentum transfers of the 200 MeV 55° and 75° measurements, respectively. The two sets of the measurements were used to separate the spectra into longitudinal and transverse components, as described below.

III. ANALYSIS

Measured typical spectra are shown in Fig. 1. These raw spectra were unfolded for radiative corrections, using the same iterative procedure²¹ applied previously in the case of ^{208}Pb . The absolute cross sections were determined by comparison with the elastic scattering cross section of ^{24}Mg , which was obtained by phase shift calculation using a Fermi-type charge distribution:

$$\rho_{gr}(r) = \rho_0 \left\{ \exp[(r - c_0)/z_0] + 1 \right\}^{-1}, \quad (1)$$

where the ground state parameter $c_0 = 2.94$ fm and $z_0 = 0.53$ fm (Ref. 22) were used in the present analysis.

It is well known that the differential form factor for excitation energy ω can be written

$$\begin{aligned} |W(q, \omega)|^2 &= \frac{d^2\sigma}{d\Omega d\omega} / \sigma_M \\ &= \frac{q_\mu^4}{q^4} |W_L(q, \omega)|^2 \\ &\quad + \left(\frac{q_\mu^2}{2q^2} + \tan^2 \frac{\theta}{2} \right) |W_T(q, \omega)|^2, \end{aligned} \quad (2)$$

where $W_L(q, \omega)$ and $W_T(q, \omega)$ are the longitudinal and transverse differential form factors, respectively, q_μ the four-momentum transfer, q the three-momentum transfer, θ the scattering angle,

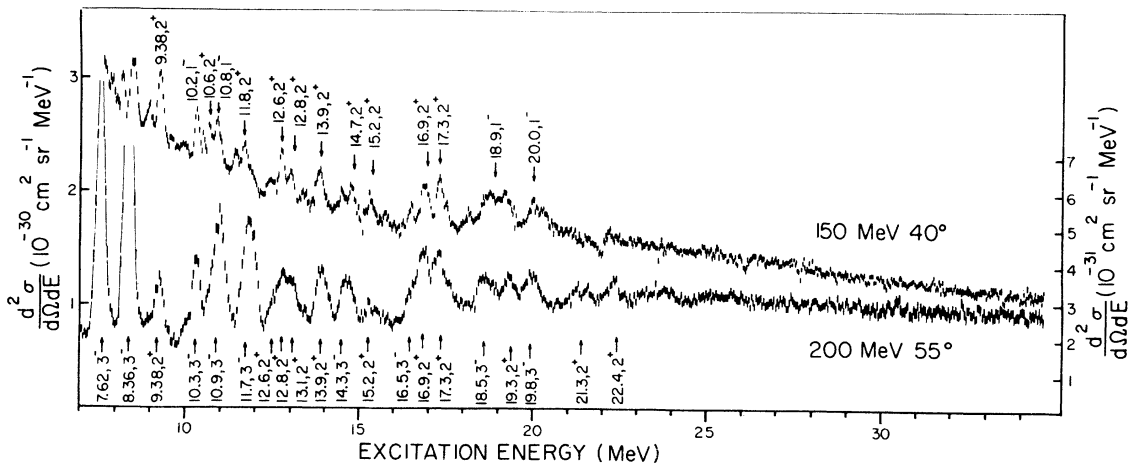


FIG. 1. Typical scattered electron spectra from ^{24}Mg obtained at 150 and 200 MeV incident electron energy and scattering angles of 40° and 55° , respectively. The right-hand scale is for the 200 MeV spectrum, and the left-hand scale for the 150 MeV spectrum.

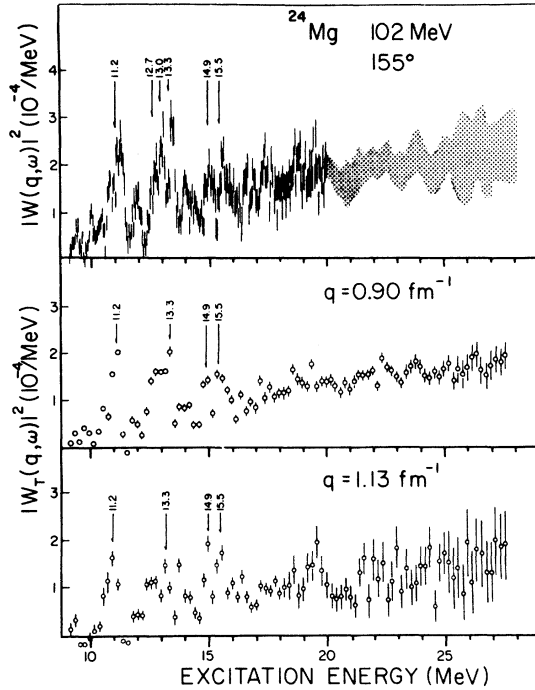


FIG. 2. The spectra for backward scattering and the transverse components. Top: spectrum obtained by 102 MeV electrons through 155° . The shaded area above 20 MeV excitation energy is the envelope of the measured points. Middle: the transverse component with energy width $\Delta\omega = 200$ keV at $q = 0.90 \text{ fm}^{-1}$, obtained by matching- q measurements at 102 MeV 155° and 200 MeV 55° . Bottom: same at $q = 1.13 \text{ fm}^{-1}$ from data at 125 MeV 155° and 200 MeV 75° .

and σ_M the Mott cross section for charge Z nucleus. The usual form factor $|F(q)|^2$ is related to the differential form factor $W(q, \omega)$ by

$$|F(q)|^2 = \int |W(q, \omega)|^2 d\omega. \quad (3)$$

A. Transverse excitation

As the principal aim of this experiment was to study the longitudinal (Coulomb) transitions, most of the measurements were performed at relatively forward scattering angles. However, since some contribution from the transverse excitations is expected even at such forward angles, spectra were also measured at a backward angle of 155° with incident energies of 102 and 125 MeV. Figure 2 shows the spectrum at 102 MeV, and the transverse components separated using Eq. (2) for 200 keV energy bin widths. The transverse component was found to be approximately 2% of the total spectrum at 200 MeV 55° , and 13% at 200 MeV 75° . As seen in Fig. 2, a general feature of the transverse

spectra is a gradually increasing cross section with increasing excitation energy. Moreover, several peaks are clearly seen at 11.2, 12.7, 13.3, and 14.9 MeV in the transverse spectra. These peaks are magnetic multipole transitions, and they are most likely $M2$, $M3$, $M2$, and $M4$ transitions, respectively.²³ The peak identified here at 15.5 MeV is the $M6$ transition,²⁴ recently observed by electroexcitation at backward angle. $M1$ transitions reported at 9.85, 9.97, and 10.7 MeV in Ref. 25 are hardly seen in these spectra because the momentum transfer region investigated here is beyond the maximum of the $M1$ form factor.

The transverse form factors integrated up to 34 MeV are shown as open circles in Fig. 10. The dash-dotted curve is the result of a calculation using the Fermi-gas model²⁶ with a Fermi momentum $k_F = 235 \text{ MeV}/c$.²⁷ The momentum transfer dependence of the transverse form factors appears to be reproduced fairly well by the transverse part of Fermi-gas model, as discussed previously.⁸ The contributions of the transverse excitations of the other forward angle spectra were estimated by interpolations or extrapolations from the spectra of Fig. 2 using the q dependence of the Fermi-gas model. The pure longitudinal spectra were thus obtained by subtracting these transverse components according to Eq. (2).

B. Multipole expansion

The various multipolarities contributing to the longitudinal spectra have been disentangled using the method of least squares, which was applied and discussed in the analysis for the giant resonance regions in ^{20}Ne (Ref. 8) and ^{208}Pb .²¹ In this method, it is assumed that the continuum spectra including resonances can be divided into small energy intervals of width $\Delta\omega$. At present each spectral bin with $\Delta\omega = 300$ keV has been expanded into longitudinal dipole ($C1$), quadrupole ($C2$), octupole ($C3$), and higher multipole excitations $\sum C_l$ ($l \geq 4$) as follows:

$$|W_i(q_i, \omega_k)|^2 = \sum_{l=1}^{\infty} a_l |X_l(q_i, \omega_k)|^2, \quad (4)$$

where the a_l 's are coefficients to be determined by the method of least squares, and the X_l 's are the momentum transfer dependences assumed for each multipole transition. The q dependence of the Goldhaber-Teller model was used for the dipole excitation and that given by the Tassie model was used for the other multipole excitations. The radial transition charge density of these models for the multipolarity l is expressed by

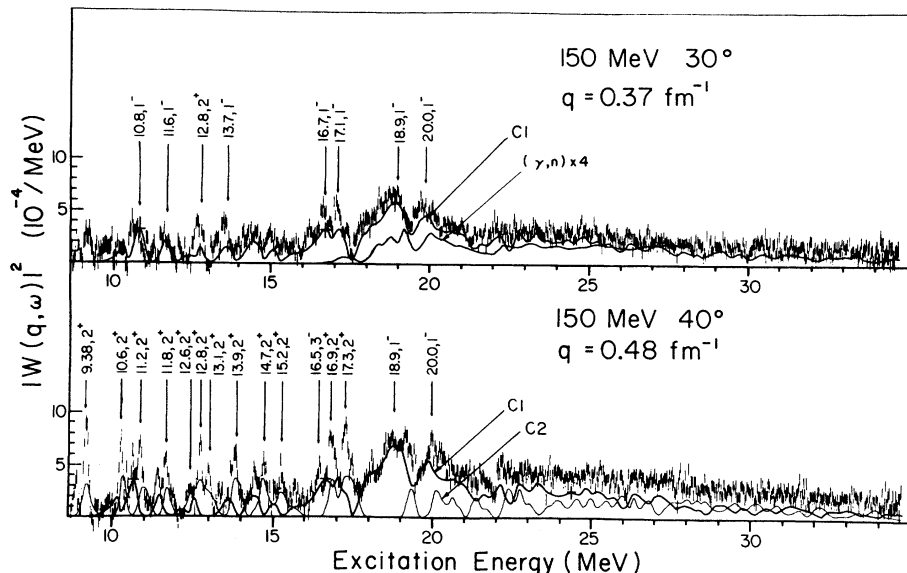


FIG. 3. The radiatively corrected spectra of ^{24}Mg at various momentum transfers as well as the results of the multipole expansion. The region of momentum transfer is favorable for dipole transition. The (γ, n) cross section of Ref. 14 was projected out to $q = 0.37 \text{ fm}^{-1}$, as described in the text.

$$\rho_{\text{tr}}(r) = r^{l-1} \frac{d\rho_{\text{gr}}(r)}{dr}, \quad (5)$$

where $\rho_{\text{gr}}(r)$ is the ground state charge density. The q dependence of the composite form factor for the higher multipole excitations was obtained in such a way that each higher multipole transition exhausts the corresponding isoscalar EWSR.

The results of the multipole expansion are shown in Figs. 3-6, together with the radiatively cor-

rected spectra. The reduced χ^2 were of the order of unity in all cases. Smoothed curves were obtained from the multipole expansions overlapping with the first expansion shifted by 150 keV. The longitudinal form factors of the various peaks with a decomposition into $C1$, $C2$, $C3$, and $\sum C_l$ ($l \geq 4$) are shown in Figs. 9 and 10. These experimental form factors were directly obtained from the spectra without assuming any nuclear continuum

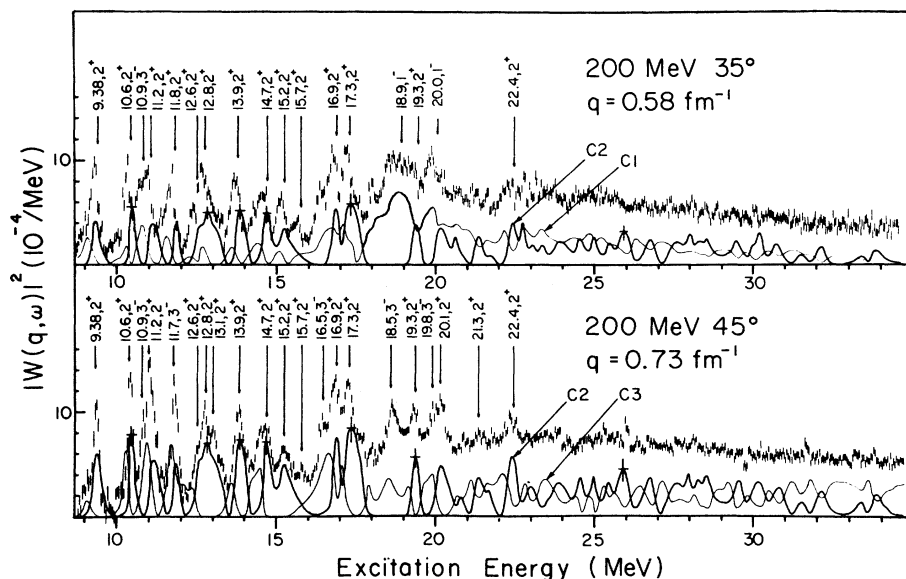


FIG. 4. See caption to Fig. 3. The region of momentum transfer is favorable for quadrupole transitions.

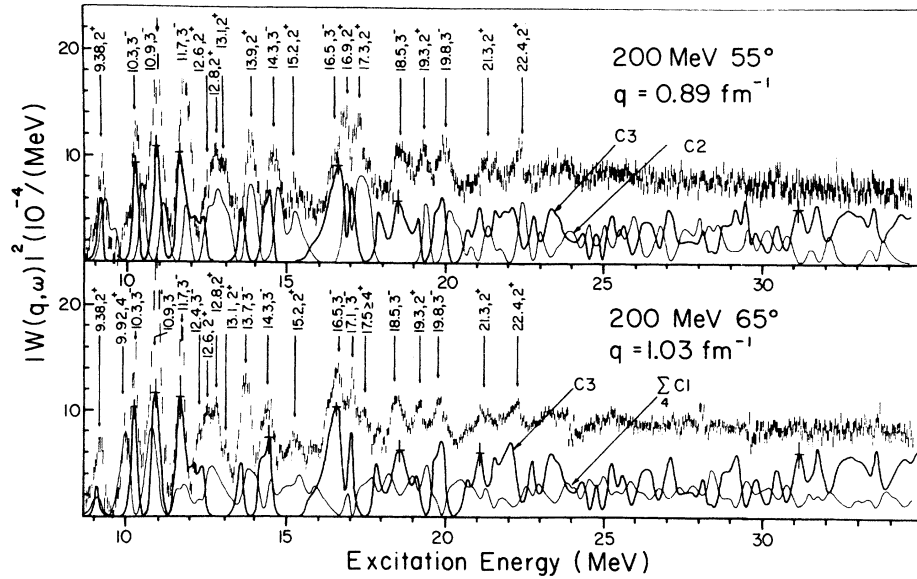


FIG. 5. See caption to Fig. 3. The region of momentum transfer is favorable for octupole transitions.

underlying resonances.

The corresponding reduced transition probabilities $B(Cl)$ obtained and the depletion of the EWSR are presented in Tables I-III. The isoscalar EWSR S_1 is given by²⁸

$$S_1 = \sum \omega B(Cl, \omega) = \frac{l(2l+1)^2 \hbar^2 Z^2}{4\pi 2M A} e^2 \langle r^{2l-2} \rangle, \quad (6)$$

where

$$\langle r^{2l-2} \rangle = \int_0^\infty r^{2l-2} \rho(\vec{r}) d\vec{r}.$$

The dipole isovector EWSR S_1 is given by

$$S_1 = \frac{9}{4\pi} \frac{\hbar^2 NZ}{2M A} e^2. \quad (7)$$

S_1 is related to the classical dipole sum \sum_c by

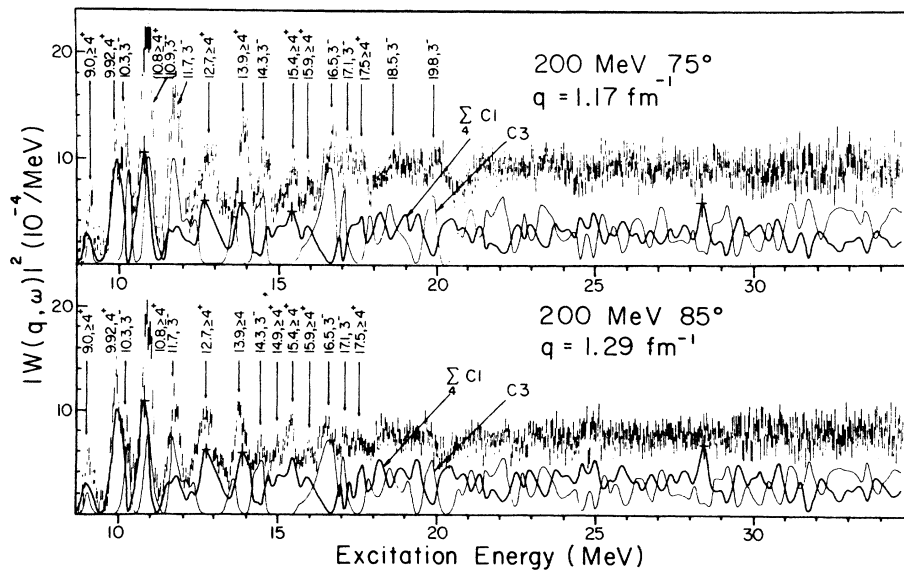


FIG. 6. See caption to Fig. 3. The region of momentum transfer is favorable for hexadecapole transitions.

$$\sum_c = \frac{16\pi^3}{9} \frac{1}{\hbar c} S_1 = 60 \frac{NZ}{A} \text{ mb MeV}. \quad (8)$$

Since the nuclear deformation may have substantial effects on the highly excited resonances, its effects on the multipole expansions have been investigated using the model developed by Suzuki and Rowe.²⁹ Their theory is based on the model independent sum rule, and the dipole and quadrupole transition charge densities are expressed in terms of the deformation parameters β_2 and β_4 . For simplicity, only the dipole and quadrupole

transition charge densities for the $K=0$ component are given here:

$$\rho_{tr}^{(1,0)}(r) \propto \left[\frac{d\rho_0(r)}{dr} + \frac{2}{\sqrt{5}} \left(\frac{d}{dr} + \frac{3}{r} \right) \rho_2(r) \right], \quad (9)$$

$$\rho_{tr}^{(2,0)}(r) \propto r \left[\frac{d\rho_0(r)}{dr} + \frac{2}{7} \sqrt{5} \left(\frac{d}{dr} + \frac{3}{2r} \right) \rho_2(r) + \frac{6}{7} \left(\frac{d}{dr} + \frac{5}{r} \right) \rho_4(r) \right], \quad (10)$$

where

$$\begin{aligned} \rho_0(r) &= \sqrt{4\pi} \left[1 + \frac{C}{4\pi} \sum |\beta_\lambda|^2 c_0 \frac{\partial}{\partial r} + \frac{1}{4\pi} \sum |\beta_\lambda|^2 c_0^2 \frac{\partial^2}{\partial r^2} \right] \rho_{gr}(r), \\ \rho_2(r) &= \left[-\beta_2 c_0 \frac{\partial}{\partial r} + \frac{1}{2\sqrt{4\pi}} \left(\frac{2\sqrt{5}}{7} \beta_2^2 + \frac{12}{7} \beta_2 \beta_4 + \frac{20\sqrt{5}}{77} \beta_4^2 \right) c_0^2 \frac{\partial^2}{\partial r^2} \right] \rho_{gr}(r), \\ \rho_4(r) &= \left[-\beta_4 c_0 \frac{\partial}{\partial r} + \frac{c_0^2}{2\sqrt{4\pi}} \left(\frac{2\sqrt{5}}{7} \beta_2^2 + \frac{200}{231} \beta_2 \beta_4 + \frac{162\sqrt{5}}{1001} \beta_4^2 \right) \frac{\partial^2}{\partial r^2} \right] \rho_{gr}(r), \end{aligned}$$

with $C = 0.5c_0 \langle r^{-2} \rangle / \langle r^{-1} \rangle$. These transition charge densities can be regarded as generalizations of the Goldhaber-Teller model to include the nuclear

TABLE I. Reduced transition probabilities $B(C1, \dagger)$ and percentage of the isovector energy-weighted sum rule S_1 . The errors are +10%, -20%. The (γ, n) data were taken from Ref. 14.

E_x (MeV)	Present		(γ, n)	
	$B(C1, \dagger)$ ($e^2 \text{fm}^2$)	S_1 (%)	E_x (MeV)	S_1 (%)
9.1	0.11	1.1		
10.2	0.039	0.44		
10.8	0.10	1.2		
11.6	0.054	0.71		
13.7	0.043	0.67		
14.4	0.077	1.2		
15.0	0.026	0.45		
16.7	0.22	4.2	16.9	0.16
17.1	0.12	2.3	17.3	0.29
			17.6	0.015
			18.3	0.84
18.9(17.7-19.5)	0.75	15.9	18.8	1.1
			19.2	0.79
20.0(19.5-20.3)	0.33	7.5	20.1	2.0
			20.4	0.29
20.3-21.4	0.28	6.5	20.9	1.2
21.4-25.0	0.77	20.0	21.5	0.41
			22.4	0.27
			23.1	2.0
25.0-28.0	0.39	10.5	25.0	4.2
			27.5	3.2
			16.5-28.0	16.7
28.0-31.0	0.22	6.5		
31.0-34.0	0.16	5.8		
9.0-34.0	3.69	84.9		

deformation.²⁹ In the present analysis, the deformation parameters $\beta_2 = +0.45$ and $\beta_4 = -0.06$ were adopted.³⁰ Figure 7 shows the predicted dipole form factors for $K=0, 1$, and the quadrupole form factor for $K=0, 1$, and 2.

Since the quadrupole form factors for $K=0$ and $K=1$ have almost identical q dependence, only four sets of the combinations were searched in the expansion with $[K(\text{dipole}), K(\text{quadrupole})] = (0, 0), (0, 2), (1, 0), \text{ and } (1, 2)$, using the same form factors for the octupole and higher multipole form factors. The shaded area of Fig. 8 shows the envelope of the results of using these four combinations. As can be seen in the figure, the spectral shape of the multipole components did not vary much as a consequence of this procedure, in spite of the different q dependence of the form factors for different K numbers.

The result of the multipole expansion indicates that almost all peaks in the spectra are a composite of different multiplicities. For instance, two bumps between 16.1 and 17.9 MeV are interpreted as a composite of dipole excitations at 16.7 and 17.1 MeV, quadrupole excitations at 16.9 and 17.3 MeV, and octupole excitations at 16.5 and 17.1 MeV. To investigate this feature of the data further, the form factors were also obtained after subtracting a phenomenological continuum shape³¹ with functional dependence of $a(\omega - \omega_0)^{1/2}$, to account for the continuum or quasielastic scattering underlying resonances. Some of the form factors obtained are shown as triangles in Figs. 9 and 10. These form factors cannot be explained by a pure multipolarity, but strongly suggest a superposition of at least two multipole excitations.

TABLE II. $B(C2, \dagger)$ and percentage of the isoscalar quadrupole EWSR S_2 . The errors are $\pm 10\%$ up to 15.7 MeV, $\pm 20\%$ above 16 MeV in excitation energy. $B(C2, \dagger)$ for the two lowest states were taken from the (e, e') work of Ref. 22. The α -particle scattering data were taken from Ref. 7. S_2 for the α -capture reaction were calculated by Bertrand *et al.* (Ref. 7) using the data of Ref. 3. The previous (e, e') data were taken from Ref. 12.

E_x (MeV)	Present		(α, α')		(α, γ_0)		(e, e')	
	$B(C2, \dagger)$ ($e^2\text{fm}^4$)	S_2 (%)	E_x (MeV)	S_2 (%)	E_x (MeV)	S_2 (%)	E_x (MeV)	S_2 (%)
1.37	446	13.3					1.37	12.4
4.23	22.8	2.1					4.23	2.4
7.34	0.9	0.2						
9.38	9.4	1.9					9.30	2.4
10.6	7.6	1.7						
11.2	9.7	2.4					11.38	0.6
11.8	6.8	1.8						
12.6	20.0	5.6					12.52	0.6
12.8			12.8	3.5	12.8	4.0	12.99	0.6
13.1			13.1	3.6	13.1	2.8		
13.9			13.9	3.0	13.9	0.4		
13.9	11.3	3.4	13.9	3.0	13.9	0.4		
14.7	10.7	3.4	14.5	3.3				
			14.9	2.5				
15.2	11.0	3.7						
15.7						15.8	0.6	
			16.6	2.3	16.5	1.1		
16.9	7.5	2.7	17.0	5.3				
17.3	19.0	7.1	17.4	8.4	17.4	1.2		
			17.8	3.1				
			18.2	2.5	18.2	0.5		
19.3	6.3	2.6	18.8	4.8				
			19.1	2.0				
			19.6	5.2				
20.1	10.0	4.3	20.0	2.3	20.0	1.0		
			20.4	6.8				
20.8	2.1	0.9	21.1	(2.7)				
21.3	7.8	3.6	21.4	(2.8)				
22.4	8.4	4.1	21.7	5.4				
22.7–25.0	20.6	10.1	24.0	7.9				
25.0–28.0	29.4	17.0						
28.0–31.0	28.5	18.3						
31.0–34.0	10.0	7.0						
0–34.0	705	117						

IV. RESULTS AND DISCUSSION

A. Results and comparison with other experiments

The results of the present analysis will be discussed in this section peak by peak and compared with other experimental results with special emphasis on the quadrupole and octupole states. The high-lying quadrupole and octupole states of ^{24}Mg have been recently studied extensively by inelastic scattering of ^3He particles¹¹ up to 11.5 MeV in excitation energy, by inelastic electron scattering¹² up to 14 MeV, and by 70 MeV α -particle scattering¹⁰ up to 19 MeV. Recent measurements using 120 MeV α particles⁷ have covered almost the entire giant resonance region up to 27 MeV. Some

of the other experimental results are compared with the present results in Tables I–III.

(i) *The 9.4 MeV peak* contains transitions to the 9.1 MeV 1^- , 9.38 MeV 2^+ states, and a higher multipole component ($\sum l \geq 4$). An $E2$ transition has also been reported at around 9.30 MeV in the (e, e') (Ref. 12), (p, p') (Ref. 9), $(^3\text{He}, ^3\text{He}')$ (Ref. 11) reactions, and in the recent analysis³² of the 120 MeV α -particle scattering data of Ref. 7. The present result of $9.4 \pm 1.0 e^2 \text{fm}^4$ is in agreement with the $11.7 \pm 1.8 e^2 \text{fm}^4$ in the (e, e') reaction of Ref. 12, in contrast with the strengths of $5.9 e^2 \text{fm}^4$ and $3.5 e^2 \text{fm}^4$ reported in the $(^3\text{He}, ^3\text{He}')$ and the recent analysis of (α, α') studies,³² respectively.

(ii) *The 9.92 MeV peak* is almost a single resonance, and the form factor indicates a hexadeca-

TABLE III. $B(C3, \uparrow)$ and percentage of the isoscalar octupole EWSR S_3 . The errors are $\pm 10\%$ up to 16.5 MeV, $\pm 25\%$ above 17 MeV. $B(C3)$ for the lowest two states were taken from previous (e, e') work of Ref. 12. The result of the (p, p') was taken from Ref. 9.

E_x (MeV)	Present		(p, p')	
	$B(C3, \uparrow)$ $10^3 e^2 \text{fm}^6$	S_3 (%)	E_x (MeV)	S_3 (%)
7.62	1.33	5.3	7.616	4.99
8.36	1.90	8.2	8.356	4.26
9.1	0.04	0.2		
10.3	0.26	1.4		
10.9	0.47	2.7	11.157	1.24
			11.318	0.31
11.7	0.71	4.3	12.016	0.58
12.4	0.24	1.5	12.261	0.39
			12.663	0.39
			12.850	0.30
				0.77
			13.344	0.33
			13.440	0.60
13.7	0.21	1.5		
14.3	0.31	2.3		
16.5	0.78	6.6		
17.1	0.18	1.6		
17.9	0.18	1.7		
18.5	0.36	3.5		
19.1	0.13	1.3		
19.8	0.34	3.5		
20.7	0.12	1.3		
21.1	0.23	2.5		
21.6	0.20	2.2		
22.0	0.42	4.8		
22.8	0.18	2.1		
23.4	0.41	4.9		
23.9-25.0	0.26	3.3		
25.0-28.0	1.04	9.3		
28.0-31.0	0.92	14.1		
31.0-34.0	1.51	25.5		
0-34.0	12.7	115		

pole transition as shown in Fig. 9. No 4^+ state has been reported in the literature³² so far at this excitation energy.

(iii) The 10.3 MeV peak essentially consists of an $E2$ transition at 10.6 MeV and an $E3$ transition at 10.3 MeV. The 2^+ state was also reported at 10.35 MeV with a strength of $11 e^2 \text{fm}^4$ in the $(^3\text{He}, ^3\text{He})$ reaction,¹¹ and at 10.36 MeV with $5.1 e^2 \text{fm}^4$ in the (α, α') reaction.³² The present result of $7.6 \pm 0.8 e^2 \text{fm}^4$ is comparable to these results. A 2^+ doublet at 10.32 and 10.35 MeV was also observed in the (p, p') reaction⁹ with a strength of $12.9 e^2 \text{fm}^4$. The 3^- state may correspond to the state identified as 4^+ at 10.35 MeV in the (e, e') reaction.¹²

(iv) The 10.9 MeV peak includes transitions to 11.2 MeV 2^+ , 10.9 MeV 3^- , and 10.8 MeV $l \geq 4$

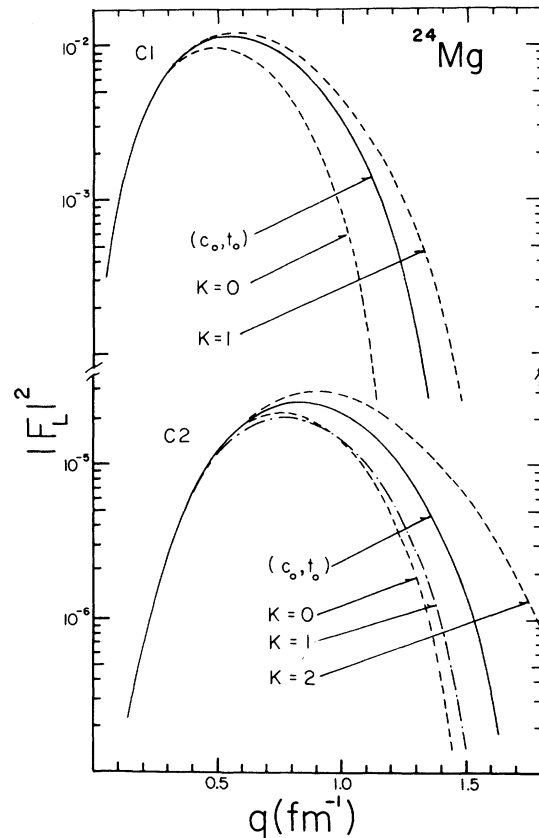


FIG. 7. Dipole and quadrupole form factors for the different K numbers as well as Tassie model (c_0, t_0) for ^{24}Mg .

states. A triplet at 11.0 MeV was observed by the (e, e') reaction¹² from which 10.93 MeV has been assigned as 2^+ . The 2^+ states at 10.92 and 11.01 MeV were also observed by the (p, p') reaction.⁹ In the (e, e') and the $(^3\text{He}, ^3\text{He})$ reactions,¹¹ octupole transitions were found at 11.1 MeV with strengths of $620 e^2 \text{fm}^6$ and $320 e^2 \text{fm}^6$, respectively, which can be compared with the present value of $470 \pm 47 e^2 \text{fm}^6$. Also a 3^- state at 11.19 MeV with a strength of $310 e^2 \text{fm}^6$ was reported in the (α, α') reaction.³²

The present result shows a large contribution from the higher multipole component at 10.8 MeV. The (p, p') experimental result also indicated $l=4$ transitions at 10.57, 10.65, and 10.82 MeV. The present analysis shows, in addition, a contribution from the dipole transition at 10.8 MeV.

(v) The 11.7 MeV peak is made up from transitions to 11.8 MeV 2^+ and 11.7 MeV 3^- states. No quadrupole transitions were reported in the (e, e') reaction. On the other hand, 2^+ states at 11.96 and 11.99 MeV were observed in the (p, p') reac-

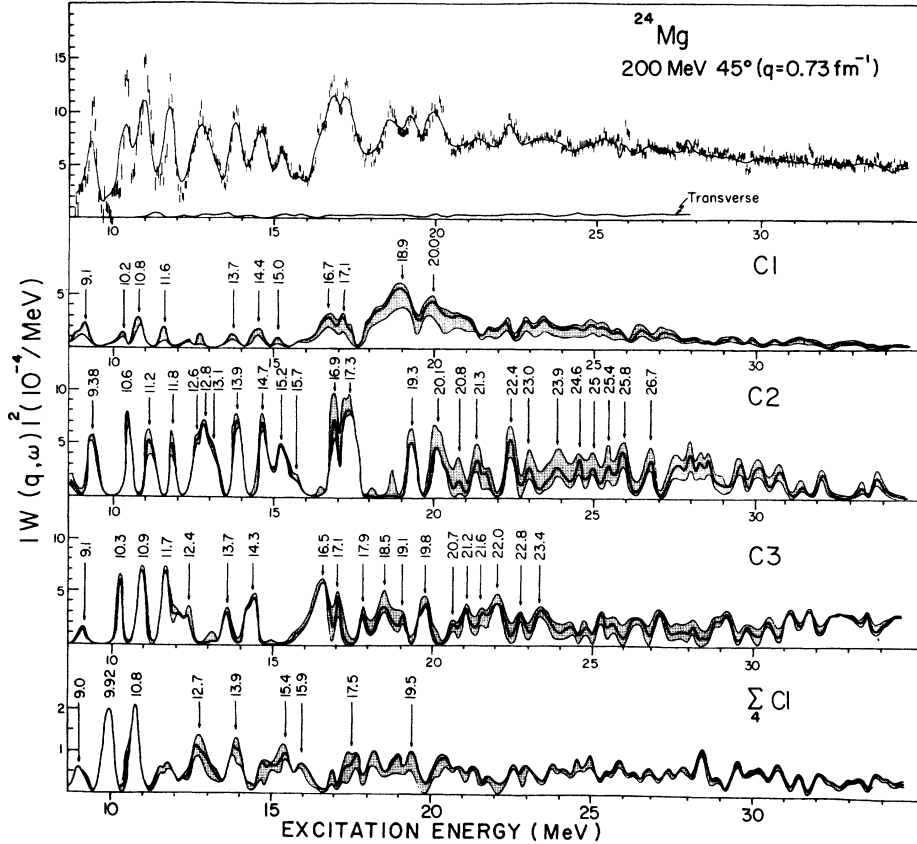


FIG. 8. Results of the multipole expansion for 200 MeV 45°. Top: radiatively corrected inelastic spectrum. The solid curve is the sum of the multipole components plus the transverse excitation. Lower part: decomposition of the spectrum into longitudinal dipole (C1), quadrupole (C2), octupole (C3), and multipoles higher than hexadecapole [$\sum C_l (l \geq 4)$]. The solid curves show the result of the decomposition using the Goldhaber-Teller and Tassie models. Dotted areas indicate possible deviations due to the combinations of the form factors of $K=0,1$ for the dipole, and $K=0, 1, \text{ and } 2$ for the quadrupole excitations.

tion, but the extracted sum strength of $3.8 e^2 \text{fm}^4$ is lower than the presently obtained value of $6.8 \pm 0.7 e^2 \text{fm}^4$. The recent analysis of the (α, α') reaction³² shows 2^+ states at 11.51 and 11.70 MeV with a sum strength of $9.2 e^2 \text{fm}^4$. In the (e, e') reaction,¹² states were observed at 11.86, 11.99, and 12.39 MeV. All these transitions display an octupole q dependence, of which the sum strength of $480 e^2 \text{fm}^6$ for the former two transitions is comparable with the present result of $710 \pm 70 e^2 \text{fm}^6$. The reported octupole strength of $93 e^2 \text{fm}^6$ at 12.01 MeV from the (p, p') reaction⁹ is far lower than this value.

(vi) *The 12.7 MeV peak.* As can be seen in Figs. 3–6 and Fig. 8, this broad bump is clearly a composite of at least four transitions; $E2$ transitions at 12.6, 12.8, and 13.1 MeV, and an $E3$ transition at 12.4 MeV. The 2^+ states with a large transverse contribution have been reported at 12.52 and 12.99 MeV in the (e, e') reaction.¹² Notice,

however, that the quadrupole strengths obtained here are extracted by a decomposition of the longitudinal excitations. In the (p, p') reaction,⁹ 2^+ states were found at 12.40, 12.47, 12.57, 12.73, 12.81, 13.08, and 13.18 MeV with a total strength of $21.3 e^2 \text{fm}^4$, which is in good agreement with the strength of $20.0 \pm 2.0 e^2 \text{fm}^4$ determined here. This is also in agreement with the (α, α') reaction,⁷ where 2^+ states were identified at 12.8 and 13.1 MeV, with some contribution from hexadecapole transitions. An octupole transition is found at 12.4 MeV in the present analysis. However, the result of the (p, p') reaction indicates several $l=3$ states in this energy region. The present analysis also indicates a possible 4^+ state at 12.7 MeV. The 4^+ states were reported at 12.50 and 12.64 MeV by the (p, p') reaction.

(vii) *The 13.8 MeV peak* is composed of 13.9 MeV 2^+ , 13.7 MeV 3^- , and 13.9 MeV, $l \geq 4$ states. The observed position and the strength of 11.3

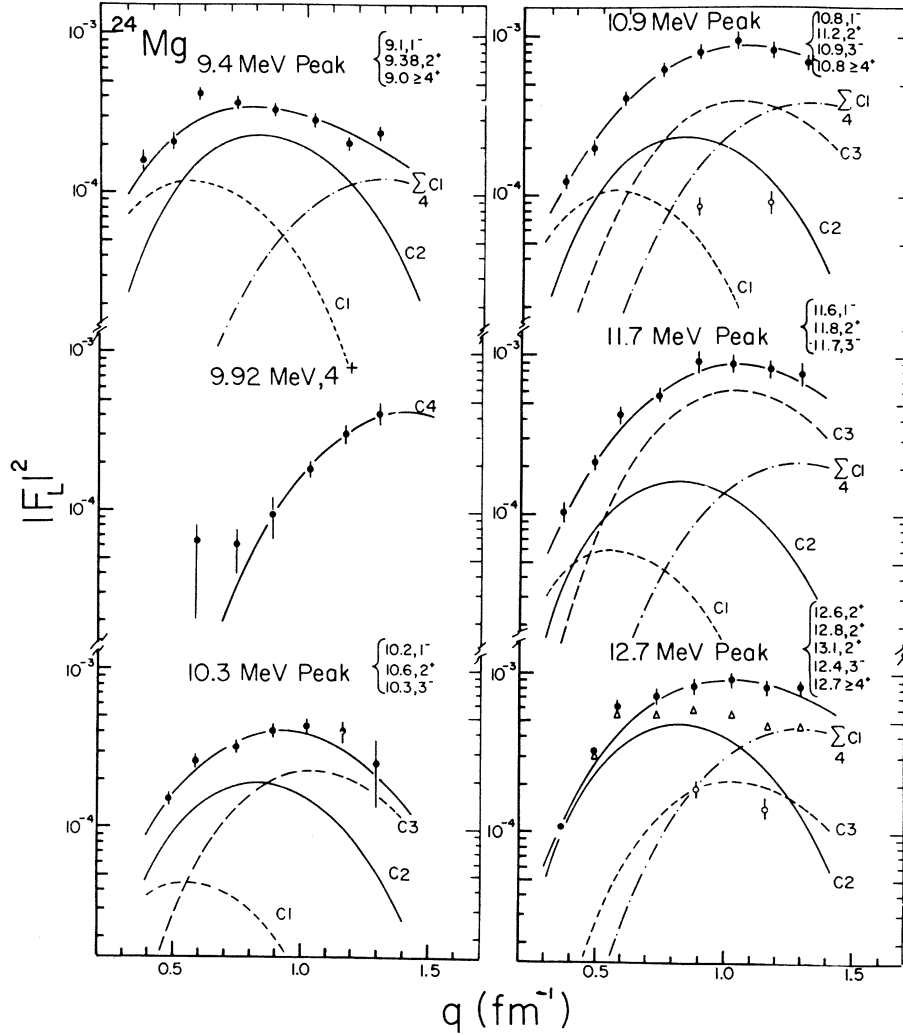


FIG. 9. Longitudinal form factors as decomposed according to the multipole expansion. Open circles indicate the contributions of the transverse excitations. The triangles are the form factors obtained by subtracting the phenomenological shape for the underlying continuum, as described in the text.

$\pm 1.0 e^2\text{fm}^4$ for the 13.9 MeV $E2$ transition is in good agreement with the (α, α') reaction.⁷ A recent analysis however suggests³² $E0$ nature for this transition.

(viii) The 14.7 MeV peak consists of transitions to 14.7 MeV 2^+ and 14.3 MeV 3^- states. Our $B(C2)$ value of $10.7 \pm 1.1 e^2\text{fm}^4$ is in agreement with the total strength of $13.3 e^2\text{fm}^4$ reported for $E2$ transitions at 14.5 and 14.9 MeV in the (α, α') reaction.^{7,32}

(ix) The region of 14.8–16.1 MeV comprises transitions to 15.2 MeV 2^+ and higher multipole excitations at 15.4 and 15.9 MeV. The 15.2 MeV 2^+ state was also reported in the (α, α') experiment by Yang *et al.*¹⁰ The recent analysis of the (α, α') reaction³² indicates three hexadecapole

transitions; however, no quadrupole states were reported in this energy region.

(x) The region of 16.1–17.9 MeV is a dipole resonance dominant at low momentum transfers. The present results show 2^+ states at 16.9 MeV ($7.5 \pm 0.7 e^2\text{fm}^4$) and 17.3 MeV ($19.0 \pm 2.0 e^2\text{fm}^4$), and 3^- states at 16.5 and 17.1 MeV. The 2^+ states were observed at 16.6, 16.9, 17.4, and 17.8 MeV in the (α, α') reaction,^{7,32} of which the 16.9 and 17.3 MeV levels agree with the present assignment of 2^+ . The sum strength of $23.3 e^2\text{fm}^4$ agrees with the present results.

(xi) The region of 17.9–20.5 MeV is dominated by the giant dipole resonance at 18.9 and 20.0 MeV. In addition, the present analysis shows 2^+ states at 19.3 and 20.1 MeV, and 3^- states at 18.5 and

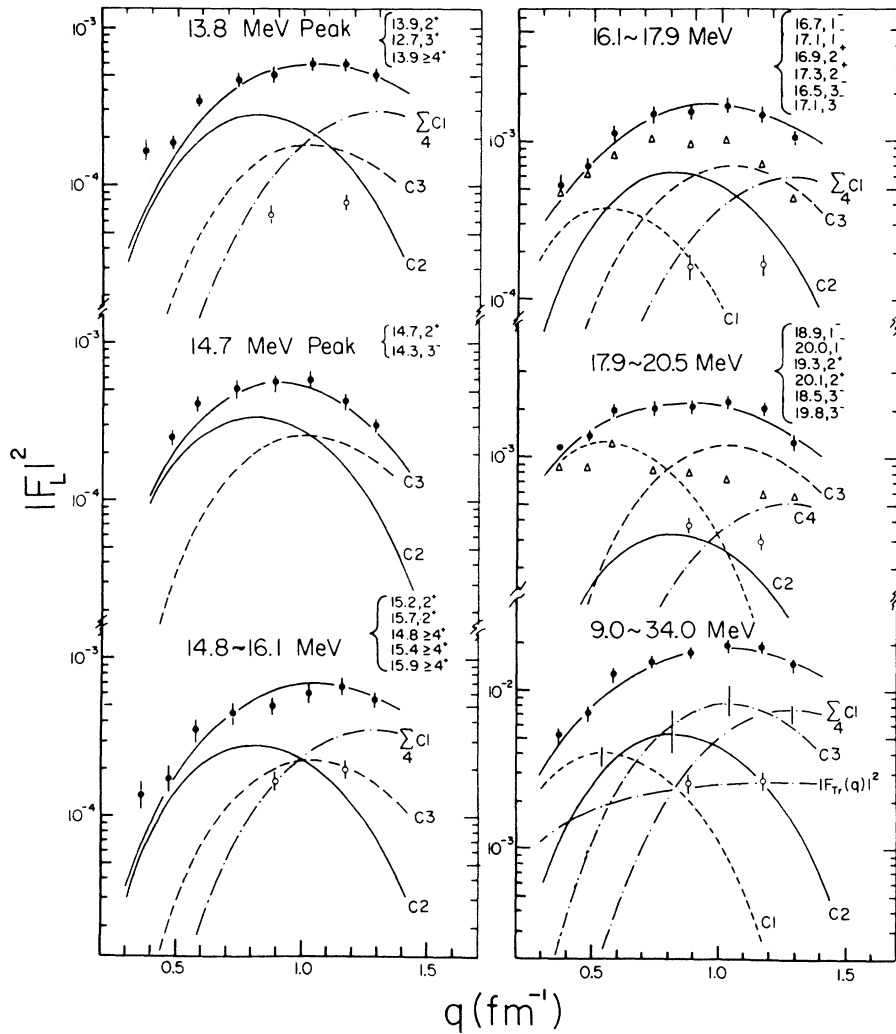


FIG. 10. See caption to Fig. 9.

19.8 MeV. The (α, α') work^{7,32} shows several 2^+ states in this region, and strength of these states amounts to $37 e^2 \text{fm}^4$. The present result indicates only two 2^+ states with a sum strength of $16.3 e^2 \text{fm}^4$. On the other hand, two octupole resonances were separated in the present analysis which do not appear in the (α, α') experimental result.

In summary, the present results for transitions from 9 to 21 MeV are generally in agreement with the available experimental results from other work, lending confidence to the validity of the method of the multipole expansion employed here. Except for the existence of octupole transitions in our data, our results are in particularly good agreement with the recent (α, α') results of Ref. 7.

B. Giant dipole resonance

Prominent dipole resonances are revealed at 16.7, 17.1, 18.9, and 20.0 MeV by the present analysis. The GDR strength exhausts 85% of the isovector dipole EWSR when integrated up to 34 MeV. The (γ, n) cross section¹⁴ is compared with the presently obtained spectrum at the lowest momentum transfer in Fig. 3. The Goldhaber-Teller model was used for the q dependence to project out the (γ, n) cross section at $q = 0.37 \text{ fm}^{-1}$. As seen in the figure, the inelastic electron spectrum at low-momentum transfer has a very similar shape to the (γ, n) cross section. The (γ, n) cross section integrated up to 28 MeV exhausts only 16% of the classical dipole sum rule,¹⁴ whereas the

present result indicates that approximately 60% of the EWSR is depleted in the same energy region. Comparison of the obtained $C1$ strength with the projected (γ, n) cross section suggests that the proton emission cross section is about 4 times larger than the (γ, n) cross section, with almost the same shape. The existing literature on the (γ, p) measurement¹⁶ also indicates that the cross section peaks around 20 MeV in excitation energy, with a magnitude about twice as large as the (γ, n) cross section.

Since ^{24}Mg is strongly deformed among sd -shell nuclei, a splitting of the GDR into at least two components corresponding to the values 0 and 1 of the quantum number K may be expected in analogy to the heavy deformed nuclei. Indeed two theoretical calculations have predicted such splitting for the GDR of ^{24}Mg . The calculation by Nilsson *et al.*,³⁴ employing the random phase approximation and Nilsson wave functions, predicts a $K=0$ component at 17 MeV and two $K=1$ resonances at between 22 and 26 MeV. Bassichis and Scheck³⁵ predict the $K=0$ resonance at 16.9 MeV and the $K=1$ resonance at 26.5 MeV, as a result of a Hartree Fock self-consistent field calculation.

In the present analysis, the χ^2 map for the different combinations of K numbers does not show any preference for the particular K numbers because of the complexities arising from other multipole transitions. However, since most of the $K=1$ strength is predicted by the theoretical calculations to lie above 20 MeV, the spreading strength at higher excitation energy (>20 MeV) in this experiment may be attributed to the $K=1$ transition.

Several additional weak dipole states between 10 and 16 MeV were identified in the present analysis. Their total strength of $0.5 e^2\text{fm}^2$ is comparable to the value found in ^{20}Ne (Ref. 8) in the same excitation energy region. The dipole states of ^{24}Mg are known to exist at 9.15, 11.39, and 11.8 MeV.³³ The (α, α') work by Yang *et al.*¹⁰ has shown that each state has a deformation parameter $\beta^2 \cong 0.0027$, which corresponds to $1.3 e^2\text{fm}^2$ of the reduced transition probability. Furthermore, the angular distributions of the 9.15 and 11.39 MeV were measured in the (p, p') experiment,⁹ from which it was concluded that these dipole transitions exhaust an appreciable fraction of the isoscalar dipole sum rule. However, the currently identified dipole transitions are isovector type, because the q dependence of the isovector dipole form factors was adopted in the multipole expansion. It is plausible to assign $1^-, T=1$ for the several peaks in the spectra at low momentum transfer, as it is noted that the $T=1$ isobaric analog states in ^{24}Mg have been identified³⁶ at

from 9.52 to 12.67 MeV excitation energy. Due to the correction of the center of mass motion, $C3$ -like q dependence for the isoscalar dipole transitions³⁷ is required in the analysis. Therefore, some possibilities of the existence of the isoscalar dipole transitions cannot be excluded among the currently identified octupole transitions.

C. Quadrupole resonance

Over twenty five quadrupole resonances could be identified by the multipole expansion. The quadrupole strength exhausts the isoscalar quadrupole EWSR when integrated up to 34 MeV. As may be seen in Fig. 8, there is considerable fragmentation of the strength between 9 and 34 MeV. In addition, a broad concentration of the quadrupole strength may exist between 19 and 31 MeV, where half of the isoscalar quadrupole EWSR is exhausted.

The present result may be compared with the inelastic electron scattering results on the adjacent nuclei ^{20}Ne ,⁸ where several prominent quadrupole peaks were found between 11 and 17 MeV, as well as a broad quadrupole excitation starting at around 17 MeV. Therefore, it may be concluded that at least for the deformed pair of sd -shell nuclei ^{20}Ne and ^{24}Mg , the GQR have similar features, namely a spreading of the resonances with relatively well defined clusters on the low energy side and a broad resonance at the higher excitations (≥ 17 MeV).

The distribution of quadrupole strength obtained here is compared in Fig. 11 to the results from α -particle scattering and α -capture reactions. The strength obtained in the present (e, e') experiment appears more spread out than the strength from the (α, α') work.⁷ Although there is an agreement between the two experiments as to the positions of strongly excited quadrupole states at 12.8, 13.1, 13.9, 16.9, 17.3, and 20.1 MeV within 100 keV, some disagreements were found in a more detailed comparison. For instance, the quadrupole states at 16.6 and 18.2 MeV observed in the (α, α') reaction were not confirmed in the present analysis, which instead indicated the existence of octupole states at 16.5 and 18.5 MeV.

It is also clear from Fig. 11 that the quadrupole strength observed in the α -capture reaction is considerably smaller than that from the (e, e') and (α, α') reactions. In the excitation energy region between 10 and 20 MeV, 33% and 50% of the EWSR are found in the (e, e') and (α, α') reactions, respectively, while only 12% of the EWSR is exhausted by the (α, γ_0) data. This fact, as suggested by Bertrand *et al.*,⁷ indicates that an appreciable fraction of the decays of the GQR

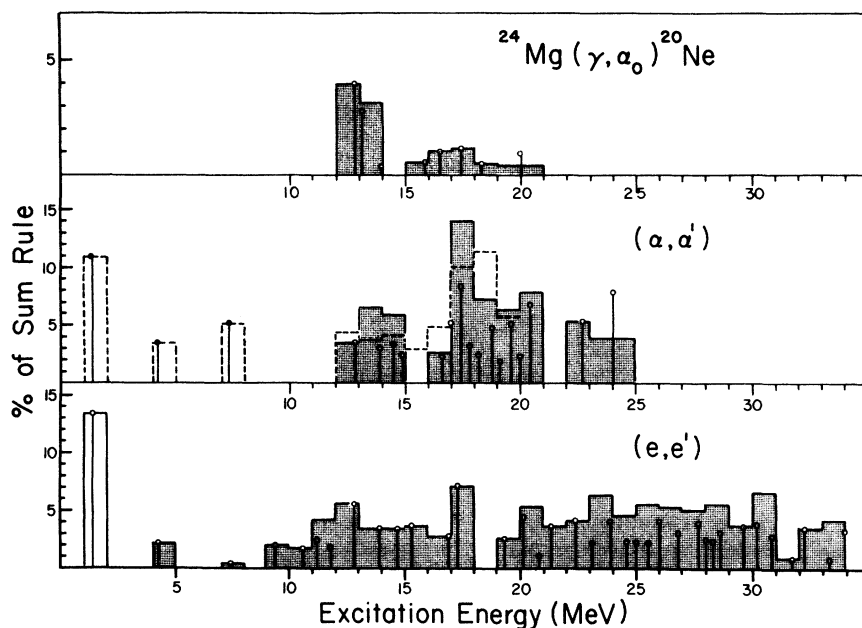


FIG. 11. Distribution of the quadrupole strength in ^{24}Mg obtained by various reactions. The strengths are shown both by lines and histograms as percentages of the isoscalar EWSR. The latter were obtained by integration over 1 MeV intervals. Top: the α_0 decay channel. The data were taken from Ref. 3. Middle: results of α scattering. The hatched area was taken from Ref. 7, whereas the dashed line was taken from the data of Ref. 10. Bottom: present (e, e') result.

occurs through other channels beside ground state alpha transition.

The spreading of the GQR in sd -shell nuclei has been also discussed in recent theoretical works. On the basis of the generator-coordinate method, Abgrall *et al.*³⁸ have found that the nuclear deformation has a dominant role in the spreading of the GQR. As shown in Fig. 12, their calculation predicts the major three components of the GQR to be at 13, 22, and 28 MeV. The present experimental result, however, apparently indicates more splitting of the GQR in ^{24}Mg . Using the rotating two-center harmonic potential, Lemmer and Toepffer³⁹ recently have shown that the quadrupole strength splits into $K=0, 1,$ and 2 components, and predicts about ten resonances in the 10 to 32 MeV excitation energy region. As seen in the comparison of Fig. 12, this calculation is in closer agreement with the data in the sense of fragmentation of the quadrupole strength. The theory also predicts³⁹ a $K=2$ transition around 26 MeV, which depletes half of the isoscalar EWSR. Since the obtained quadrupole strength amounts to half of the EWSR between 20 and 34 MeV, the major part of the quadrupole strength above 20 MeV might be attributed to the $K=2$ excitation.

D. Octupole and higher multipole resonances

One of the interesting features of our data is that approximately twenty octupole resonances

were separated between 9 and 25 MeV. Although the reduced transition probability for each octupole resonance is approximately one order of magnitude smaller than that of the well-known 7.62 and 8.36 MeV octupole states, the entire octupole strength exhausts the isoscalar octupole EWSR when integrated up to 30 MeV.

Recently nine high-lying octupole states were

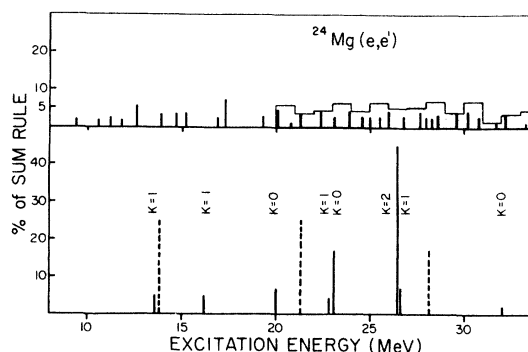


FIG. 12. Comparison with the theoretical calculations for the quadrupole strength as percentages of the EWSR. The upper part shows the present result. The quadrupole strength above 20 MeV is also shown as a histogram. The lower part shows theoretical predictions. The solid lines with K number are the results of the two-center shell model calculation by Lemmer and Toepffer (Ref. 39), and the dashed lines are the results of Abgrall *et al.* (Ref. 38).

observed by inelastic proton scattering⁹ between 11.1 and 13.5 MeV, as shown in Table III. Including strong octupole transitions at 7.61 and 8.36 MeV, the total octupole strength from such work amounts to $775 e^2\text{fm}^6$, depleting 13% of the isoscalar EWSR. The octupole strength from the present work amounts to $950 e^2\text{fm}^6$ for the same energy region. The recent analysis of the (α, α') data shows,³² on the other hand, four octupole states between 10 and 15 MeV, depleting 5% of the EWSR. Also, an upper limit of about 15% of the EWSR was reported⁴⁰ for the compact octupole group between 4 and 14 MeV in ^{27}Al . The angular distribution could be fitted in this case by a superposition of the quadrupole and octupole excitations.

Shell structure effects on the high-lying octupole states in spherical nuclei has been discussed recently.^{28,41-43} In the harmonic oscillator model, the isoscalar octupole strength is split into two components at 1 and $3\hbar\omega$, with roughly equal strength of the reduced transition probabilities.^{28,41-43} Recently observed concentrated octupole resonances at around $30/A^{1/3}$ MeV in medium and heavy nuclei were reported to exhaust in the range of $\frac{1}{2}$ to $\frac{2}{3}$ of the expected $1\hbar\omega$ isoscalar octupole strength,¹³ and thus has been interpreted as a counterpart of the collective low-lying $1\hbar\omega$ octupole transitions.

In contrast with the case of medium and heavy nuclei, the present results show that the $1\hbar\omega$ octupole transitions are distributed in a wide energy region currently studied, in addition to the two low-lying octupole states at 7.62 and 8.36 MeV. Furthermore, since $3\hbar\omega$ states are expected to be broader in the lighter nuclei,⁴³ it may be concluded that the isoscalar $3\hbar\omega$ excitations are also observed in the present experiment, especially at higher excitation energies above 20 MeV, where octupole resonances seem broader. On the other hand, because most of the isovector strength is expected theoretically above 30 MeV,^{28,42} these transitions probably constitute a nuclear continuum located beyond the excitation energies currently investigated.

Evidence for the existence of a considerable number of multipole resonances higher than hexadecapole is clearly seen in Figs. 6 and 8. These higher multipole resonance consist of C4, C5, and C6 transitions. The major part of these higher multipole resonances are considered to be hexadecapole, judging from the momentum transfer regions currently studied. As is seen in Figs. 6 and 8, several separated bumps at 9.92, 10.8, 12.7, 13.9, and 15.4 MeV were found in the spectra as well as a rather continuous part above 20 MeV in excitation energy. Among these bumps, a

relatively well-separated peak at 9.92 MeV is a C4 excitation. In Fig. 9, the q dependence for the C4-form factor was taken from the best fit form factor²² of the 6.00 MeV, 4^+ state in ^{24}Mg . The reduced transition probability $B(C4, \uparrow)$ for the state were found to be $(1.0 \pm 0.1) \times 10^4 e^2\text{fm}^6$. The strength of these higher multipole resonances are considerably large; approximately 45% of the isoscalar hexadecapole EWSR is exhausted up to 34 MeV if we assume the whole spectrum consists of only hexadecapole transitions.

Over ten $l=4$ transitions were observed between 9 and 13.5 MeV in the (p, p') reaction,⁹ exhausting 4% of the isoscalar EWSR. The positions of the multipole states with $l \geq 4$ obtained in this work do not fully agree with the (p, p') data, due in part to the fact that the present (e, e') data contain other multipole transitions higher than hexadecapole. However, the 10.8 MeV peak may correspond to the $l=4$ transitions at 10.57 and 10.65 MeV, and the 12.7 MeV peak may correspond to a combination of E4 transitions at 12.85, 12.97, and 13.05 MeV observed in the (p, p') reaction.⁹

V. CONCLUSION

The giant resonance regions of inelastic electron scattering spectra from ^{24}Mg have been decomposed into dipole, quadrupole, octupole, and higher multipole transitions by the method of least squares using appropriate q dependence for each multipole transition.

Prominent dipole resonances are revealed at 16.7, 17.1, 18.9, and 20.0 MeV. The giant dipole strength exhausts 85% of the isovector dipole EWSR. The dipole strength is spread over the whole region of excitation energy currently studied, in contrast with the theoretical predictions of a concentration of the $K=1$ dipole strength around 25 MeV.

Over twenty-five quadrupole resonances were separated between 9 and 34 MeV, which consist of relatively well resolved peaks up to 17 MeV, and a broad distribution of strength centered at around 25 MeV. These characteristics are considered a common feature of the quadrupole distribution of deformed sd -shell nuclei. The total quadrupole strength exhausts the isoscalar quadrupole EWSR.

Approximately twenty octupole resonances were, moreover, identified between 9 and 25 MeV. The octupole strength is again very much fragmented; the total strength, however, exhausts the isoscalar EWSR. The octupole transitions consist possibly of $3\hbar\omega$ excitations as well as $1\hbar\omega$ excitations. Evidence for the existence of higher multipole transitions such as hexadecapole resonances

is also found in the excitation energy region between 9 and 34 MeV.

ACKNOWLEDGMENTS

The authors wish to thank Professor A. Van der Woude and Dr. Van der Borg, who informed us of the results of the recent analysis of the (α, α') ex-

periment (Ref. 32) prior to its publication. One of the authors (K.I.) expresses his thanks to Professor E. J. Ansaldo for reading this manuscript through and making valuable comments. One of us (K.I.) was supported for this work by the Natural Sciences and Engineering Research Council of Canada, and the Laboratory of Nuclear Science, Tohoku University.

*Present address: National Laboratory for High Energy Physics, Oho-machi, Tsukuba-gun, Ibaraki-ken, Japan 305.

- ¹F. E. Bertrand, *Annu. Rev. Nucl. Sci.* **26**, 457 (1976).
²S. S. Hanna, in *Lecture Notes in Physics*, edited by S. Costa and Schaerf (Springer, New York, 1977), Vol. 61.
³E. Kuhlmann, E. Ventura, J. R. Calarco, D. G. Mavis, and S. S. Hanna, *Phys. Rev. C* **11**, 1525 (1975).
⁴J. M. Moss, C. M. Rozsa, D. H. Youngblood, J. D. Bronson, and A. D. Bacher, *Phys. Rev. Lett.* **34**, 748 (1975).
⁵K. T. Knöpfle, G. J. Wagner, A. Kiss, M. Rogge, C. Mayer-Böricke, and T. Bauer, *Phys. Lett.* **64B**, 263 (1976).
⁶A. Kiss, C. Mayer-Böricke, M. Rogge, P. Turek, and S. Wiktor, *Phys. Rev. Lett.* **37**, 1188 (1976).
⁷F. E. Bertrand, K. van der Borg, A. G. Drentje, M. N. Harakeh, J. van der Plicht, and A. van der Woude, *Phys. Rev. Lett.* **40**, 635 (1978).
⁸Z. M. Szalata, K. Itoh, G. A. Peterson, J. Flanz, S. P. Fivozinsky, F. J. Kline, J. W. Lightbody, Jr., X. K. Maruyama, and S. P. Penner, *Phys. Rev. C* **17**, 435 (1978).
⁹B. Zwieglinski, G. M. Crawley, H. Nann, and J. A. Nolen, Jr., *Phys. Rev. C* **17**, 872 (1978).
¹⁰G. C. Yang, P. P. Singh, A. van der Woude, and A. G. Drentje, *Phys. Rev. C* **13**, 1376 (1976).
¹¹R. J. Peterson and F. E. Cecil, *Nucl. Phys.* **A297**, 10 (1978).
¹²A. Johnston and T. E. Drake, *J. Phys. A* **7**, 898 (1974).
¹³J. M. Moss, D. H. Youngblood, C. M. Rozsa, D. R. Brown, and J. D. Bronson, *Phys. Rev. Lett.* **37**, 816 (1976); *Phys. Rev. C* **18**, 741 (1978).
¹⁴S. C. Fultz, R. A. Alvarez, B. L. Berman, M. A. Kelly, D. R. Lasher, T. W. Phillips, and J. McElhinney, *Phys. Rev. C* **4**, 149 (1971).
¹⁵D. V. Webb, E. G. Muirhead, and B. M. Spicer, *Nucl. Phys.* **A159**, 81 (1970).
¹⁶K. Shoda, K. Abe, T. Ishizuka, N. Kawamura, and M. Kimura, *J. Phys. Soc. Jpn.* **17**, 735 (1962).
¹⁷B. S. Dolbilkin, V. I. Korin, L. E. Lazareva, F. A. Nikolaev, and V. A. Zapevalov, *Nucl. Phys.* **72**, 137 (1965).
¹⁸O. Titze, E. Spamer, and A. Goldmann, *Phys. Lett.* **4**, 169 (1967).
¹⁹M. Sugawara, T. Ichinoe, S. Urasawa, M. Oyamada, T. Kubota, A. Kurihara, O. Konno, Y. Shibazaki, T. Terasawa, K. Nakahara, S. Nemoto, M. Muto, K. Shoda, and Y. Torizuka, *Nucl. Instrum. Methods* **153**, 343 (1978).
²⁰M. Kimura, Y. Torizuka, K. Shoda, M. Sugawara, T. Saito, M. Oyamada, K. Nakahara, K. Itoh, K. Sugiyama, M. Gotoh, K. Miyashita, and K. Kurahashi, *Nucl. Instrum. Methods* **95**, 403 (1971).
²¹M. Sasao and Y. Torizuka, *Phys. Rev. C* **15**, 217 (1977).
²²A. Nakada and Y. Torizuka, *J. Phys. Soc. Jpn.* **32**, 1 (1972).
²³T. Saito *et al.*, Research Report of Lab. of Nucl. Sci., Tohoku University, **13**, 1 (1980).
²⁴H. Zarek, B. O. Pich, T. E. Drake, D. J. Rowe, W. Bertozzi, C. Creswell, A. Hirsch, M. V. Hynes, S. Kowalski, B. Norum, F. N. Rad, C. P. Sargent, C. F. Williamson, and R. A. Lindgren, *Phys. Rev. Lett.* **38**, 750 (1977).
²⁵L. W. Fagg, *Rev. Mod. Phys.* **47**, 683 (1975).
²⁶W. Czyz, *Phys. Rev.* **131**, 2141 (1963).
²⁷E. J. Moniz, I. Sick, R. R. Whitney, J. R. Ficenc, R. D. Kephart, and W. P. Trower, *Phys. Rev. Lett.* **26**, 445 (1971).
²⁸A. Bohr and B. R. Mottelson, *Nuclear Structure* (Benjamin, New York, 1975), Vol. 2, Chap. 6.
²⁹T. Suzuki and D. J. Rowe, *Nucl. Phys.* **A292**, 93 (1977).
³⁰Y. Horikawa, Y. Torizuka, A. Nakada, S. Mitsunobu, Y. Kojima, and M. Kimura, *Phys. Lett.* **36B**, 9 (1971).
³¹Y. Torizuka, K. Itoh, Y. M. Shin, Y. Kawazoe, H. Matsuzaki, and G. Takeda, *Phys. Rev. C* **11**, 1174 (1975).
³²K. van der Borg, Ph.D. thesis, Rijksuniversiteit te Groningen, 1979 (unpublished).
³³P. M. Endt and Van der Lein, *Nucl. Phys.* **A214**, 1 (1973).
³⁴S. G. Nilsson, J. Sawicki, and N. K. Glendenning, *Nucl. Phys.* **33**, 239 (1962).
³⁵W. H. Bassichis and E. Scheck, *Phys. Rev.* **145**, 771 (1966).
³⁶S. M. Tang, B. D. Sowerby, and D. M. Sheppard, *Nucl. Phys.* **A125**, 289 (1969).
³⁷Y. Torizuka, M. Oyamada, K. Nakahara, K. Sugiyama, Y. Kojima, T. Terasawa, K. Itoh, A. Yamaguchi, and M. Kimura, *Phys. Rev. Lett.* **22**, 544 (1969).
³⁸Y. Abgrall, B. Morand, E. Caurier, and B. Grammaticos, *Phys. Rev. Lett.* **39**, 922 (1977).
³⁹R. H. Lemmer and C. Toepffer, *Nucl. Phys.* **A319**, 89 (1979).
⁴⁰C. U. Mayer-Böricke, in *Proceedings of the Sendai Conference on Electro- and Photoexcitation, 1977*, edited by Y. Kawasoe, supplement to Research Report of Lab. of Nucl. Sci., Tohoku University, **10**, 53 (1977).
⁴¹G. F. Bertsch and S. F. Tsai, *Phys. Rep.* **18C**, 125 (1975).
⁴²K. F. Liu and G. E. Brown, *Nucl. Phys.* **A265**, 385 (1976).
⁴³S. Shlomo and G. Bertsch, *Nucl. Phys.* **A243**, 507 (1975).

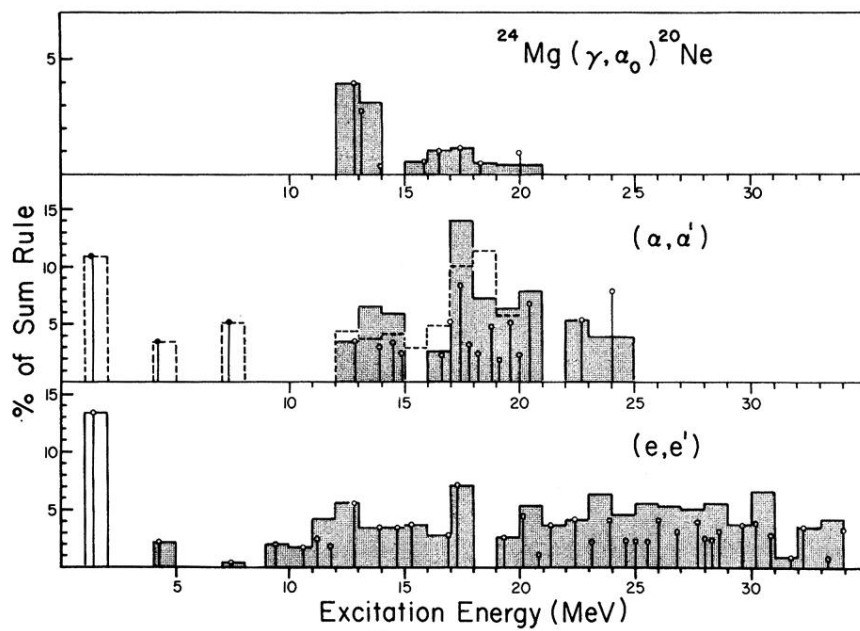


FIG. 11. Distribution of the quadrupole strength in ^{24}Mg obtained by various reactions. The strengths are shown both by lines and histograms as percentages of the isoscalar EWSR. The latter were obtained by integration over 1 MeV intervals. Top: the α_0 decay channel. The data were taken from Ref. 3. Middle: results of α scattering. The hatched area was taken from Ref. 7, whereas the dashed line was taken from the data of Ref. 10. Bottom: present (e, e') result.

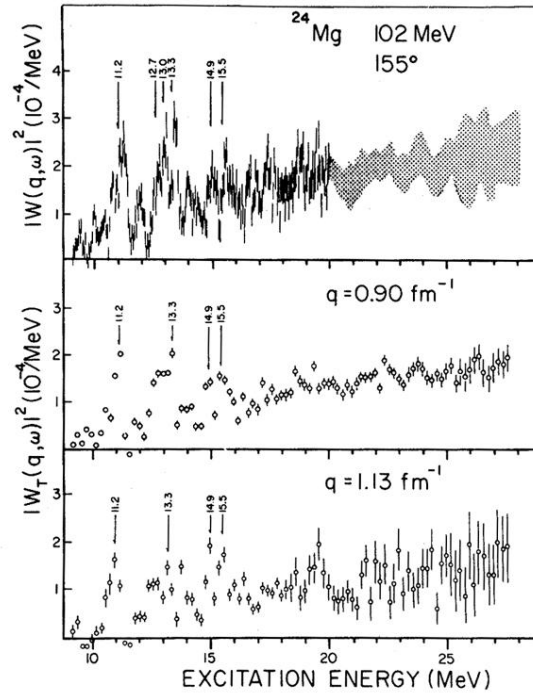


FIG. 2. The spectra for backward scattering and the transverse components. Top: spectrum obtained by 102 MeV electrons through 155°. The shaded area above 20 MeV excitation energy is the envelope of the measured points. Middle: the transverse component with energy width $\Delta\omega = 200$ keV at $q = 0.90 \text{ fm}^{-1}$, obtained by matching- q measurements at 102 MeV 155° and 200 MeV 55°. Bottom: same at $q = 1.13 \text{ fm}^{-1}$ from data at 125 MeV 155° and 200 MeV 75°.

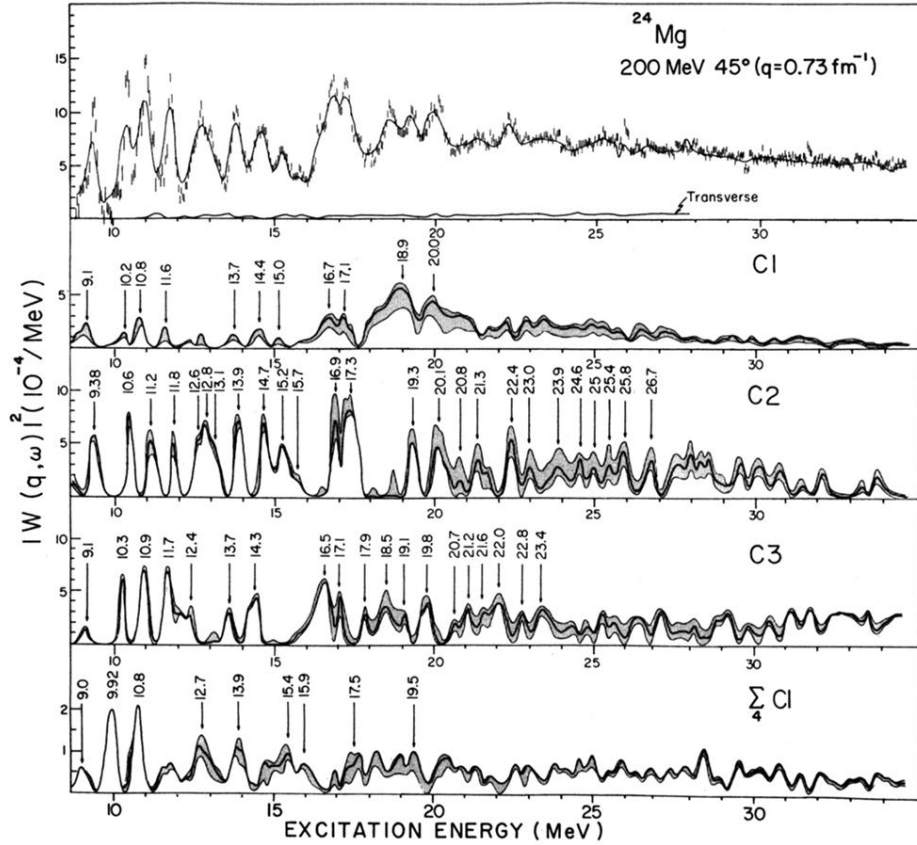


FIG. 8. Results of the multipole expansion for 200 MeV 45°. Top: radiatively corrected inelastic spectrum. The solid curve is the sum of the multipole components plus the transverse excitation. Lower part: decomposition of the spectrum into longitudinal dipole (C1), quadrupole (C2), octupole (C3), and multipoles higher than hexadecapole [$\sum C_l (l \geq 4)$]. The solid curves show the result of the decomposition using the Goldhaber-Teller and Tassie models. Dotted areas indicate possible deviations due to the combinations of the form factors of $K=0,1$ for the dipole, and $K=0, 1, \text{ and } 2$ for the quadrupole excitations.